Characterization of liver injury, oval cell proliferation and cholangiocarcinogenesis in glutathione S-transferase A3 knockout mice

Crawford, Dana R.; Ilic, Zoran; Guest, Ian; Milne, Ginger L.; Hayes, John D.; Sell, Stewart

Published in:
Carcinogenesis

DOI:
10.1093/carcin/bgx048

Publication date:
2017

Document Version
Peer reviewed version

Characterization of liver injury, oval cell proliferation and cholangiocarcinogenesis in glutathione S-transferase A3 knockout mice

Running title: GSTA3 KO mice liver injury and carcinogenesis

Dana R. Crawford[1*#], Zoran Ilic[2#], Ian Guest[2], Ginger L. Milne[3], John D. Hayes[4], and Stewart Sell[2]

[1]Albany Medical Center, Center for Immunology and Microbial Disease, 43 New Scotland Avenue, Albany, NY 12208, [2]Wadsworth Center, New York State Department of Health, Albany, NY 12201, [3]Vanderbilt University School of Medicine, Department of Medicine and Pharmacology, Nashville, TN 37323, and [4]Division of Cancer Research, Medical Research Institute, University of Dundee, Ninewells Hospital and Medical School, Dundee, Scotland, DD1 9SY

[*] To whom correspondence should be addressed. Tel: 518-262-6652; Fax 518-262-6161; Email: crawfod@mail.amc.edu

[#] These authors contributed equally to this work

Abbreviations: AFB1 – aflatoxin B1; HCC – hepatocellular carcinoma; KO – knockout; WT – wild-type; GSTA3 –glutathione S-transferase A3 subunit; CYP1A2 – Cytochrome P450 1A2; CYP3A11 – Cytochrome P450 3A11; OC – oval cell; CCA-cholangiocarcinoma.

Abstract

We recently generated glutathione S-transferase (GST) A3 knockout (KO) mice as a novel model to study the risk factors for liver cancer. GSTA3 KO mice are sensitive to the acute cytotoxic and genotoxic effects of aflatoxin B1 (AFB1), confirming the crucial role of GSTA3 in resistance to AFB1. We now report histopathological changes, tumor formation, biochemical changes and gender response following AFB1 treatment as well as the contribution of oxidative stress. Using a protocol of weekly 0.5 mg AFB1/kg administration, we observed extensive oval (liver stem) cell (OC) proliferation within 1-3 weeks followed by microvesicular lipidosis, megahepatocytes, nuclear inclusions, cholangiomas, and small nodules. Male and female GSTA3 KO mice treated with 12 and 24 weekly AFB1 injections followed by a rest period of 12 and 6 months, respectively, all had grossly distorted livers with macro- and microscopic cysts, hepatocellular nodules, cholangiomas and cholangiocarcinomas and OC proliferation. We postulate that the prolonged AFB1 treatment leads to inhibition of hepatocyte proliferation which is compensated by OC proliferation and eventually formation of cholangiocarcinoma (CCA). At low-dose AFB1, male KO mice showed less extensive acute liver injury, OC proliferation, and AFB1-DNA adducts than female KO mice. There were no significant compensatory changes in KO mice GST subunits, GST enzymatic activity, epoxide hydrolase, or CYP1A2 and CYP3A11 levels. Finally, there was a modest increase in F_2-isoprostane and isofuran in KO mice that confirmed putative GSTA3 hydroperoxidase activity *in vivo* for the first time.

Summary

We've extended characterization of our novel GSTA3 knockout mice toward better understanding human liver cancer. Our results demonstrate extensive oval cell proliferation, numerous pathological changes, tumor formation, and increased female susceptibility following aflatoxin and CCl_4 exposure in GSTA3 knockouts.

Introduction

Aflatoxin B_1 (AFB1) is a potent hepatotoxin and hepatocarcinogen for humans and most other mammalian species, but adult mice are highly resistant (1). AFB1 is produced by the mold *Aspergillus flavus*, which typically grows on groundnuts, grain and maize that are commonly consumed by mice. This dietary exposure is one reason that mice may have developed resistance to the mycotoxin. In both human and mice, AFB1 is metabolized by cytochromes P450 (CYP) to a reactive AFB1-epoxide that can cause genotoxic damage by binding with DNA at the *N*-7 atom of guanine (2). Once formed, the AFB1-epoxide may be detoxified by conjugation with reduced glutathione through the catalytic actions of members of the cytosolic family of glutathione S-transferase (GST) enzymes. The glutathione conjugates of AFB1-epoxides are excreted in urine as water soluble aflatoxin mercapturic acids (AFB1-NAC) (3). The intrinsic resistance of mice to AFB1 may be attributed to a relatively low ability of CYP isoenzymes to form the reactive epoxide and/or high ability of GST isoenzymes to form glutathione conjugates. Mice constitutively express a hepatic class Alpha GST subunit, GSTA3 (with the dimeric enzyme called A3-3), which exhibits high activity towards AFB1-epoxide and is thought to contribute to the resistant phenotype (4). Interestingly, the rat, which is sensitive to

AFB1 hepatocarcinogenesis, possesses an inducible class Alpha GST that is similar to mouse GSTA3, and when induced by chemopreventive agents confers resistance to the mycotoxin (5).

Newborn mice are substantially more susceptible to AFB1 hepatocarcinogenesis than adult animals (6). We found that newborn mice have very low hepatic GST levels and high hepatic AFB1 DNA adduction when compared to their adult counterparts (1). Thus, we hypothesized that the resistance of adult mice to AFB1 is related to the relatively high levels of expression of GSTA3. To test this, we constructed a GSTA3 knockout (KO) mouse (7). In contrast to resistant adult wild-type (WT) mice, adult GSTA3 KO mice harboring disruption of the GSTA3 gene exhibited acute cytotoxicity and genotoxicity upon exposure to AFB1. Specifically, AFB1-treated GSTA3 KO mice acquired ≥100-fold more AFB1-N^7-DNA adducts in their livers than did similarly treated WT mice, and GSTA3 KO mice died of massive hepatic necrosis at doses of AFB1 that exert minimal toxicity on WT mice (7). These results indicated that GSTA3 is a primary determinant of intrinsic resistance to AFB1 in the mouse. Importantly, humans lack a GST isoenzyme with the same high catalytic activity towards AFB1-epoxide as mouse GST A3-3. Thus, the GSTA3 KO mice may be considered “humanized” in regard to AFB1 metabolism.

Oval cells (OCs) are thought to be putative liver stem cells that may give rise to hepatocellular and cholangiocellular carcinomas (8,9). Although there are reports of induction of OC proliferation in mice (10), the extent is far less than in rats and the significance of OCs in mice in liver regeneration and as precursors of liver cancer is not clear. They are seen in human livers associated with severe tissue damage and can be

induced experimentally in several species, mostly in various models in rats and, less frequently and at very much reduced numbers, in mice (11,12). When seen in the context of carcinogen exposure, OC are thought to function as cancer stem cells that are capable of developing into hepatocellular and/or cholangiocellular carcinomas (8, 9,13). Thus, the study of OCs in animal models is important from two perspectives: 1, as cancer stem cells, as the cells of origin of liver cancer, and; 2, as normal stem cells, for their potential use in regeneration therapy.

In the present paper, we assess the effects of loss of GSTA3 on AFB1-induced toxicity by measuring histopathological changes, tumor formation, gender response, AFB1 metabolism, OC response, AFB1-DNA adduct formation, GST enzyme activity, and the extent of oxidative damage in liver tissues. Our results provide new insights into the response of our new humanized KO mouse model to carcinogen treatment toward better understanding liver cancer.

Materials and methods

Mice. Three-month old female and male GSTA3 KO mice were injected i.p. with the appropriate dosage of AFB1 or carbon tetrachloride (CCl_4) (see results for doses used in various experiments). AFB1 (Sigma-Aldrich, St. Louis, MO) was dissolved in DMSO and administered to mice in a volume of 100 µl per 30 grams body weight). CCl_4 was obtained from Sigma (≥95 5%) and administered in corn oil to final 1 ml/kg body weight. Mice were then euthanized on the appropriate days after injection of AFB1. At necropsy, liver and other tissues were collected and fixed in formalin, and then processed, embedded in paraffin, sectioned and stained with H&E. Histological evaluation of all

tissues was undertaken by Dr. Sell, a certified pathologist. All animal studies were approved by the Wadsworth Center Institutional Animal Care and Use Committee (Dr. Sell, PI; Protocol #15-370), and animals handled and treated according to the regulations set forth in the approved Wadsworth Center Institutional Animal Care and Use Protocol.

Immunohistochemistry. A6 and cytokeratin (oval cells). Formalin fixed and paraffin embedded tissues were cut at 5 µm and antigens retrieved by immersing slides in trypsin buffer (0.1% trypsin, 0.1% $CaCl_2$ in PBS) with addition of proteinase K (25 µg/ml) for 15 minutes at 37°C. Tissues were then treated with 0.3% hydrogen peroxide in 100% methanol for 15 minutes and blocking serum (3% normal goat serum in PBS containing 1% BSA) for 30 minutes before adding primary monoclonal rat anti-mouse A6 antibodies (a gift from Dr. Valentina Factor, NIH) diluted 1:10 and incubated overnight at 4°C. The next day, peroxidase was blocked with 3% hydrogen peroxide for 10 minutes before adding secondary goat anti-rat biotinylated antibody for 60 minutes at room temperature (1:100 dilution, Jackson Immuno Research). Extravidin-peroxidase (1:400 dilution; Sigma) was added for 30 minutes at room temperature, followed by color development with 3,3'-diaminobenzidine (DAB), counterstaining with hematoxylin, dehydration in ethanol and xylenes, and mounting in Permount. Between each step, tissues were rinsed in PBS. Labeling for wide spectrum cytokeratin (CK) was done identically to A6 staining except for the following: 1) antigen retrieval was done with trypsin but without addition of proteinase K; 2) primary antibody was rabbit anti-bovine cytokeratin (1:100 dilution, Dako). **Albumin, Hep-Par1 and GST-P (hepatocytes).** Stainings were done identically to that described above for cytokeratin and A6, except

that 1) antigens were retrieved by boiling tissues (at 95-100ºC) in citrate buffer (pH 6) for 40 minutes and 2) Hep-Par1 and GST-P incubation with primary antibody was for 1 hour at room temperature. The primary antibodies used were: rabbit anti-albumin, 1:100 dilution (Sigma), rabbit anti-Hep-Par1, 1:80 dilution (Sigma) and anti-GST-P (placental glutathione S-transferase), 1:1000 dilution (MBL Co.).

Histochemistry. Mucicarmine staining was done on formalin fixed and paraffin embedded tissues cut at 5 µm. Slices were stained with hematoxylin for 10 minutes, washed and then soaked in muciramine solution (Sigma) for 1 hour at room temperature. Slides were then washed, counterstained in metanil yellow for 1 min, dehydrated and coverslipped in Permount. **GGT** (γ-glutamyl transpeptidase) histochemistry was done on frozen sections cut at 10 µm and fixed in cold acetone for 10 minutes. They were then incubated in solution containing GGT substrate GMNA (L-glutamic acid γ-(4-methoxy-ß-naphtylamide, Sigma), glycyl-glycine and Fast Blue BB salt for 20 min and stained in cupric sulfate for 2 min as described (14).

AFB1-DNA adduct analysis. AFB1-N^7-guanine adducts were measured in liver tissue using liquid chromatography-electrospray ionization tandem mass spectrometry as previously described (7). Values were expressed as pmol/mg DNA.

Liver extract preparation. Four groups of 3-month old C57Bl/6J mice representing WT male, WT female, GSTA3 KO male, and GSTA3 KO female (7 animals each) were sacrificed and the livers saline perfused, removed, and snap frozen in liquid nitrogen. At the time of processing, the frozen tissues were added to ice-cold lysis buffer (Cell Signaling, Danvers, MA) containing phosphatase and protease inhibitors and sonicated, centrifuged 20 minutes at 11,000 x *g*, and the supernatant extract collected.

GST purification. The liver 11,000 x *g* supernatants were chromatographed on a glutathione-agarose affinity column and bound GST proteins eluted, all according to the manufacturer (Novagen/EMD Millipore, Billerica, MA). These samples were then concentrated using Amicon Ultra 4 columns (EMD Millipore) and protein concentration in these concentrates determined using the BioRad protein reagent (BioRad).

GST enzyme activity. The GST enzymatic activity in the glutathione-agarose affinity purified liver supernatants were quantified using a GST assay kit, which utilizes 1-chloro-2,3-dinitrobenzene as the substrate, according to the manufacturer (Sigma). These analyses were carried out using 0.2 µg protein per well after first establishing that this was in the linear portion of velocity curve.

F2-Isoprostane and isofuran oxidation marker analyses. Snap frozen liver tissues were analyzed by the Vanderbilt University Eicosanoid Core Laboratory using gas chromatography and mass spectroscopy as previously described (15). Values were expressed as ng per gram liver tissue (ng/g).

Western blot analyses. Equal amounts of protein (2.5 µg) per well were electrophoresed on a 14% SDS PAGE gel, transferred to nitrocellulose, and allowed to react with various GST antibodies (16). These antibodies included 1:2,000 dilutions of rabbit antiserum against GSTA3, GSTA4, and GSTM5 as well as 1:3,000 dilutions of rabbit antiserum against GSTM1 and GSTP1. Antisera probings were successive and separated by blot stripping to remove cross-reacting antibodies from the previous reaction using the Restore Plus Western blot stripping buffer (ThermoFisher, Waltham, MA). After incubation with primary antibody and appropriate washes to eliminate non-specific binding, the immobilized protein on the blots were allowed to react with a goat

anti-rabbit secondary HRP conjugate (1:2000) and washed again. The antibody signal was then captured using the Western lightning plus kit substrate (PerkinElmer, Waltham, MA) and the resultant chemiluminescent signal was captured by film, and quantified using ImageJ software.

Cytochrome P450 and epoxide hydrolase analyses. Western blots were exposed to primary antibodies against CYP1A2 (Santa Cruz Biotechnology, Dallas, TX), CYP3A11 (EMD Millipore), and microsomal epoxide hydrolase (Detroit R&D, Detroit, MI), and then processed as described above. Signals were normalized to VDAC1 after stripping.

Liver function analysis. Aspartate transaminase (AST) was measured from serum samples taken at each time point as described (17) by the Molecular Diagnostics laboratory of Wadsworth Center using a Roche cobas 6000 analyzer.

Statistics. Data are reported as the mean +/- SEM with statistical significance defined as $p<0.05$ using a 2-tailed Student's *t*- test.

Results

Tumor formation in GSTA3 KO mice in response to AFB1 exposure. Male and female mice were treated once per week with 0.5 mg/kg AFB1 for 12 (4 males, 6 females) and 24 (5 males, 7 females) weeks and livers analyzed at 12 and 6 months, respectively, after the last AFB1 injection. Mice that received 24 injections had a rest period of 8 weeks between the first 12 and last 12 injections. All mice had grossly distorted livers, with cysts, nodules and tumors, with 24 injections resulting in more numerous and coalescing lesions than 12 injections (Figure 1A-D). Histologically, these

lesions are hepatocellular nodules (mostly of the early or Becker type 1 grade) (18), cholangiomas and cholangiocarcinomas (Figure 1E-M). Two serial sections of the largest diameter of each lobe were examined. All examined mice have multiple cholangiomas; 2/4 males and 3/6 females given 12 injections, and 3/5 males and 7/7 females given 24 injections had cholangiocarcinomas; and 2/4 males and 3/6 females given 12 injections and 5/5 males and 7/7 females given 24 injections have from one to three Becker type 1 hepatocellular nodules (and only occasionally a Becker type 2 or 3 nodule). There are no hepatocellular carcinomas (Becker type 4 nodules) or distant metastases (e.g. lung). There is normal liver histology in all vehicle (DMSO) treated control mice (5 males and 5 females, 12 and 24 weekly injections). In addition to their typical morphology, the identity of cholangiomas and cholangiocarcinomas is confirmed by cells staining positive for pan-CK and for mucin (mucicarmine stain) (Figures 1J and 1K). Hepatocellular nodules are best identified by morphology. Some hepatocyte foci are positive for GGT (Figure 1L), but so are some small cholangiomas as well as many individual cells, hepatocytes and, based on typical shape and proximity to cholangiomas and cholangiocarcinomas, oval cells. GST-P also does not stain hepatocellular nodules, only some individual hepatocytes and some small foci of hepatocytes (Figure 1M). Anti-albumin and anti-Hep-Par1 immunohistochemistry label most normal hepatocytes but nodules show mixed positive and negative cells (data not shown).

Histologic effects of AFB1 treatment in GSTA3 KO mice. The detailed histopathologic changes seen over time during treatment of male and female GSTA3 KO mice with AFB1 (3-5 mice/time point) are shown in Figure 2 using a protocol of weekly (1-12) 0.5 mg AFB1/kg administration. Tissues from 4 to 8 mice of both sexes

were evaluated for each time. Megahepatocytes were counted in 10 random 200X fields and expressed as number of cells per field. Due to the difficulty in accurately counting oval cells, as they can show as either single cells or as part of ductules, they were scored (from 0 to 4+) according to the following criteria: Grade 0 - there are less than 5 oval or duct-like cells beyond the immediate periportal zone; Grade 1+ - up to 20 oval cells are seen extending into the first 1/3rd of the liver lobule but not in all lobules; Grade 2+ - 20 to 100 oval cells extend into the mid-lobule but not to the central vein; Grade 3+ - 100-300 oval cells extend to the central vein in essentially all lobules, but many hepatocytes are still seen; Grade 4+ - Greater than 300 oval cells make up most of the cells of the lobule. At 1-3 weeks, oval cell proliferation (0-1+) is seen (Figure 2B,C) and this increased throughout the period of observation as compared with untreated mice (Figure 2A). At 3-5 weeks there is massive hepatocyte microvesicular lipidosis, involving the entire lobule in all mice (Figure 2D) and oval cells are prominent in both males and females (2+ to 4+). No megahepatocytes are present. By 6-8 weeks, OC proliferation continues to be high (grades 2+ to 4+) but the microvesicular fatty change is replaced by large hepatocytes (megahepatocytes) (Figure 2E) with eosinophilic cytoplasm and large nuclei (males: 1.6±0.7/field; females: 2.0±0.8/field) and nuclear inclusions are first seen (Figure 2F). At 9-12 weeks, megahepatocytes continue to be prominent (males: 1.7±2.4/field; females: 1.3±0.9/field) as are nuclear inclusions. There are now cholangiomas (Figure 2G) and small grade I nodules in a few mice (Figure 2H). At 3-4 months after last (12^{th}) weekly AFB1, megahepatocytes are spread throughout most of the parenchyma (males: 13.3±9.6/field; females: 9.6±14.0/field) with prominent nuclear inclusions. There are multiple peripheral cholangiomas almost all

mice. At this time, only half of both males and females had one or two type 1 hepatocellular nodules.

Female GSTA3 KO mice are more sensitive to acute AFB1 exposure than male GSTA3 KO mice. To assess and compare the response of our KO mice to acute AFB1 in both genders, female and male GSTA3 KO mice were injected i.p. with a single dose of AFB1 and 4 to 9 mice euthanized at 5, 10, 15, 30, 60 and 90 days after administration of the mycotoxin. Oval cell proliferation was quantified by grading the tissues from 0 to 4+, as described above. At the highest single AFB1 dose in female KO mice (1.0 mg/kg), there is fat accumulation, cell necrosis and swelling after 5 days (Figure 3B) and oval cells are present in small numbers (graded from 0 to 1+; grade average 0.7±0.4 per mouse). OCs increase significantly by day 10 (2+ - 4+; grade average 2.8±1.4) (Figure 3C,D) and day 15 (1+ - 3+; grade average 1.8±0.7) (Figure 3E) after administration of AFB1. The reduction in numbers of OCs at day 15 compared to day 10 is due to greater variability among 8 mice examined at this time point. OCs peak again around day 30 (2+ - 4+; grade average 2.9±0.8) (Figure 3F) and then decrease between days 60 (0 – 1+; grade average 0.6±0.6) and 90 (almost no OC present in any animal). The OCs typically form single files or narrow ductules around hepatocytes and extend throughout the liver lobule from the portal to the pericentral zone. They stain positive with antibodies against oval cell/bile duct specific markers A6 (Figure 3G) and pan-cytokeratin (PanCK; Figure 3H).

In contrast to females, male GSTA3 KO mice have no liver injury after 1.0 mg/kg AFB1 injection and no OC regenerative response (Figure 3I). Following repeated dosing, however, the livers of GSTA3 KO males display similarly extensive OC

proliferation as did females. Female and male GSTA3 KO mice injected with vehicle (DMSO; Figure 3A for female) and WT mice injected with the same doses of AFB1 have no injury (data not shown for WT mice).

Female KO mice exhibit higher AFB1-DNA adduct levels. Previous studies demonstrated a striking increase in the levels of AFB1-N^7-guanine adducts in GSTA3 KO versus WT male mice (7). In the present study, these previous analyses were extended to assess comparative gender response. Analyzing adducts as previously described (7), female KO mice develop 3.5-fold more adducts than male KO mice (183.2 pmol/mg DNA vs. 52.7 pmol/mg DNA) when given 0.87 mg/kg AFB1 by gavage (Figure 4).

KO mice, especially females, exhibit decreased GST isoform expression. To further investigate the basis behind the observed gender differences, we examined the possible compensatory response of other GST subunits in male versus female KO mice using glutathione affinity column-purified samples and Western immunoblotting. As expected, no GSTA3 was detected in livers of KO mice (Figure 5A). We also examined GSTP1, GSTM1, GSTM5 and GSTA4 levels in mouse liver. Overall, no compensatory up-regulation of these other GST isoforms was observed in GSTA3 KO mice. Remarkably, an overall reduction in one of the most abundant mouse GST subunits (GSTP1) was observed in KO livers (Figure 5B). In addition, we discovered a greater decrease in GSTP1 in KO female than in KO male mice (Figure 5B. Note: this was further confirmed by running these samples on the same blot; data not shown). Statistically significant reductions in the expression of GSTM5 (Figure 5D) but not GSTA4 (Figure 5E) were detected in both male and female KO as compared with WT

mice. Thus no overall GST subunit compensatory increase occurs in GSTA3 KO mouse liver. In fact, there is a reduction of the GSTP1 subunit, which is even more pronounced in female KO mice than in male KO mice.

CYP1A2 but not CYP3A11 or microsomal epoxide hydrolase levels were increased in male KO mice. We also assessed the levels of cytochrome P4501A2 (CYP1A2), P4503A11 (CYP3A11, the main mouse equivalent of human CYP3A4), and microsomal epoxide hydrolase, major proteins involved in aflatoxin metabolism as part of phase 1 response that regulate aflatoxin epoxide levels (19-21) in liver extracts. Levels of CYP1A2, which contributes to aflatoxin epoxide formation, were significantly higher in KO males as compared with WT males or either female genotype (Figure 5F). However, this increase is not likely to be compensatory since a compensatory effect would instead be expected to be a reduction of CYP1A2 in KO mice as a way of reducing substrate activation. This CYP1A2 signal was also much more variable than other proteins analyzed thus far. Levels of cytochrome CYP3A11, which also contributes to aflatoxin epoxide formation, also exhibited significant variability but statistically, did not show a difference in WT versus KO or in male versus female mice (Figure 5G). In addition, there were no differences in the levels of microsomal epoxide hydrolase, an enzyme that can hydrolyze and detoxify AFB1, in WT versus KO or in male versus female mice (Figure 5H).

Glutathione S-transferase (GST) activity is higher in WT males. Total GST activity was assessed in glutathione affinity column-purified eluate. Values were similar in males and females except for a significantly increased level in WT males (Figure 5I). This increase in GST activity in livers of WT male mice likely reflects both the presence

of GSTA3 (versus knockouts) as well as much higher levels of GSTP1 in WT males versus KO males or WT and KO females. Importantly, and specific to aflatoxin, we have also previously reported that urinary excretion of AFB1-NAC, a product of glutathione adduction of AFB1 that is mediated by GSTs, is dramatically reduced in GSTA3 KO versus WT mice (22).

KO mice show increased oxidation in response to CCl_4. Oxidative stress damage was also assessed in WT versus KO mice based on the fact that many liver carcinogens (including AFB1) are also oxidants (23-25), and also because GSTA3 exhibits *in vitro* peroxidase activity toward the substrate cumene hydroperoxide (26). The relative importance of GSTA3 in a cellular antioxidant defense has never been directly tested *in vivo*, and as such, our KO mice represent a first opportunity to address this. In order to readily assess and compare strong enough signals, we used the potent liver oxidant carbon tetrachloride (CCl_4), which was also used for a similar purpose to assess GSTA4 peroxidase activity *in vivo* (27). Mice were administered 1 ml/kg CCl_4 and at appropriate time points, the lipid peroxidation markers F_2-isoprostanes and isofurans were measured. As shown in Table 1, almost all F_2-isoprostane and isofuran levels are greater – in some cases statistically significantly so – in GSTA3 KO versus WT mice following exposure to CCl_4. Overall, there is a modest increase in F_2-isoprostane and isofuran oxidation markers in KO mice. This also confirms predicted GSTA3 peroxidase activity *in vivo* for the first time.

Regarding gender-dependent sensitivity, there were greater constitutive as well as induced F_2-isoprostane levels in female GSTA3 KO mice at 24 hours compared with male KO mice. This also occurred at 24 hours for isofuran. However, the reverse

occurred at 8 hours. Overall, we conclude that there is a modest increase in oxidative stress damage in female- as compared to male-KO mice.

There were also significant changes in the ratios of F_2-isoprostane to isofuran levels at 2 and 8 hours independent of genotype and gender. Interestingly, levels of F_2-isoprostanes and isofurans are much greater two hours after CCl_4 exposure when compared with the commonly used 24 hour time point, suggesting that a 24 hour time point is less sensitive if not inadequate for assessing CCl_4-stimulated oxidative damage *in vivo*.

Hepatocellular damage increases with exposure time to CCl_4, and does not correlate with peak oxidative damage. The release of the liver function marker AST into serum was also evaluated after CCl_4 exposure. As shown in Table 1, a statistically significant increase in serum AST occurred at 8 hours and especially 24 hours. These results are consistent with the damaging effects of CCl_4, since AST is a liver damage marker. Interestingly, AST levels did not correlate with lipid peroxidation markers F_2-isoprostanes and isofurans (Table 1). Specifically, lipid peroxidation peaked at 2 hours and fell almost completely back to control levels after 24 hours of CCl_4 exposure, whereas AST release was maximal at 24 hours.

Discussion

Since AFB1 is a major risk factor for HCC in humans, GSTA3 knockout (KO) mice were constructed to provide a mouse model for the study of AFB1 carcinogenesis. As hoped, these mice exhibited acute cytotoxicity and genotoxicity upon exposure to AFB1, establishing these knockouts as a useful model to study the interplay of risk factors

leading to liver injury and cancer development in humans (7). Here, we extend these studies to better understand this mouse model and to provide new insights into human liver cancer.

Using various aflatoxin and oxidative stress protocols, we assessed histopathological changes, tumor formation, key biochemical changes and gender response in detail. Most notably, there is extensive oval (OC) proliferation which increases over time. This is followed by microvesicular lipidosis, megahepatocyte-, nuclear inclusion-, and cholangioma-, and small nodule-formation, providing detailed morphological characterization of pathological responses to AFB1. After long term exposure to AFB1 all mice display severely distorted livers with cysts, nodules and tumors, identified histologically as hepatocellular nodules and cholangiomas and cholangiocarcinomas. Because GSTA3 KO are the first, and only, mice made that are sensitive to AFB_1, no protocol was available as a guide on the dose and regimen of AFB_1 to use. The commonly used regimen of AFB1 exposure in rats, daily injections for 4-8 weeks, results in hepatocellular foci and HCC, without cholangiomas (28,29). The GSTA3 KO mice cannot survive a similar daily regimen, but the total dose of AFB1 given to mice (6-12 mg/kg) in our long term exposure is similar to that used in rats. The association of AFB1 and development of CCA has been reported before. For example, chronic exposure of hamsters to AFB1 results in tumors of CCA and mixed HCC/CCA types (30). Also, rats exposed to AFB1 develop CCA (or mixed hepatocholangiocellular carcinomas) if AFB1 is combined with agents that induce OC proliferation (a carcinogen 2-acetylaminofluorene + partial hepatectomy) (31). The association between proliferating oval cells and resulting cholangiocarcinomas, and suggestion of a possible

causative link between the two, has been reported in other models of liver cancer in rats (32,33), mice (34) and hamsters (35) as well as in humans (36,37).

The OC response in KO mice – especially female - was much greater and different in growth pattern than in other mouse models reported in the literature. There are several ways to induce OCs in mouse liver, from employing certain chemicals to spontaneous induction in transgenic or knockout mice. However, the majority of reports rely on two models: DDC (3,5-diethoxycarbonyl-1,4-dihydrocollidine) supplemented diet (38,39), and less frequently, CDE (choline deficient/ethionine) supplemented diet (40,41). Both of these models induce a relatively low level ductular-type OC response, do not induce tumors, and neither agent is relevant for human health. In contrast, the OC proliferation that we describe here in GSTA3 KO mice is associated with the clinically relevant environmental carcinogen (AFB1), is sustained over many weeks, is much more severe, is morphologically different from DDC or CDE (not ductular), and may result in development of neoplastic liver lesions. Thus, our GSTA3 KO mouse represents a valuable model for studying the role of OCs in normal liver regeneration and in liver tumor development.

In essentially all susceptible species studied including humans, rats and trout, males have a much greater toxic and carcinogenic susceptibility to AFB1 than females (1). Thus, we expected a similar gender effect in GSTA3 KO mice. Surprisingly, however, male KO mice exhibited significantly less acute liver injury, OC proliferation, and AFB1-DNA adduct levels than female KO mice when exposed to a single low dose of AFB-1. We considered the possibility that male KO mice have a greater compensatory response to loss of GSTA3 than female KO mice, and thereby express higher levels of

other transferases. However, instead of an increase in other GST subunits, there was an overall reduction of the most abundant isoforms (GSTP1 and GSTM1) in both male and female KO mice. Additionally, there was lack of a significant epoxide hydrolase, CYP1A2, CYP3A11 or GST specific activity compensatory response in the KO mice although an increase of CYP1A2 was seen in male but not female mice. Overall, these results provide evidence that initial susceptibility to AFB1 is greater in female mice, however this increased female susceptibility disappears with repeated exposures.

Besides detoxifying AFB1, GSTA3 is notable for possessing glutathione peroxidase activity toward organic hydroperoxides (26)**.** GSTA3 has a functional antioxidant response element (ARE) in its gene promoter (42), and is induced in a nuclear factor-erythroid 2 p45-related factor 2 (Nrf2)-mediated fashion following treatment with phenolic antioxidants or cytoprotective compounds. The relative importance of GSTA3 in a cellular antioxidant defense has never been directly tested *in vivo*. AFB1 exposure leads to a pro-oxidant state and redox analysis is directly relevant to AFB1 carcinogenesis (21-24). Pro-oxidants are known mutagens (43-45), and thus may contribute, in addition to AFB1-DNA adducts, to AFB1 liver carcinogenesis. We assessed oxidative damage in GSTA3 KO mice using CCl_4, which is well known for its ability to produce centrolobular necrosis of the liver; has been used extensively in studies of the proliferation of hepatocytes after liver injury (46) including in our laboratory (47). It has been used for a similar purpose to assess GSTA4 peroxidase activity *in vivo* (27). CCl_4 liver injury is thought to mainly involve generation of reactive oxygen species (ROS), including lipid hydroperoxides (48), and has been frequently used as an inducer of ROS in mice. Overall, we observed a modest increase in F_2-

isoprostane and isofuran oxidation markers in KO mice, providing evidence – for the first time – that GSTA3 possesses peroxidase activity *in vivo*. We also observed greater F_2-isoprostane and isofuran in females than males. The GST A4-4 isoenzyme also reduces organic hydroperoxides, and its expression has been linked to AFB1 toxicity in mice (49). Mice lacking GSTA4 exhibit increased levels of 4-hydroxynonenal (4-HNE) as compared with their WT counterparts (27,49). Most of the increase in 4-HNE was present constitutively in these previous studies, with little increase after oxidative stress. Conversely, we observed significant differences between WT and KO mice in the oxidative marker levels under constitutive conditions and also after treatment with CCl_4.

Interestingly, our detailed time course analysis found peak oxidation at time points that were quite distinct (i.e., much earlier) from published studies. These results indicate the best time points to assess oxidation using CCl_4, and perhaps other oxidants; not just for our study but also as a guide for other researchers in the field. Also of interest was the difference between peak oxidation (2 hours) and peak liver function enzyme release (24 hours). The latter 24-hour peak might be one reason why researchers have chosen to assess oxidative damage after 24 hours, but we demonstrate here that the two effects are temporally distinguishable. The long delay between peak oxidative damage and peak serum AST also suggests that lipid peroxidation leads to subsequent and time-consuming stress response signaling before eventual AST release. This interpretation is consistent with a growing list of lipid peroxidation products such as 4-HNE that have been identified as important cell signalers (50).

In conclusion, we have extended characterization of our novel GSTA3 KO mouse model. This includes assessing the sequence of events leading up to and including histopathological changes, tumor formation, biochemical changes and gender response following AFB1 treatment as well as the contribution of oxidative stress. Our results also provide evidence that initial susceptibility to AFB1 is greater in female mice, in contrast to the known higher rate of liver cancer in males in humans, and that oval cell response and GSTA3 peroxidase activity may influence susceptibility to cancer development.

The repeated long term exposure of the GSTA3 KO mice to AFB1 leads to marked long-lasting proliferation of OCs and eventually hepatocellular nodules, cholangiomas and CCAs. Exposure of rats to diethylnitrosame does not induce proliferation of OCs and results in HCC (8,9). In other rat models with extensive OC proliferation early HCC appear later after the carcinogen exposure has been discontinued (8,9). This may allow OC differentiation to hepatocytes and then these “induced” hepatocytes form HCC. Thus, in hepatocarcinogenic models where OC proliferation is greatest and hepatocyte proliferation is inhibited, it appears that CCA is induced rather than HCC.

Funding

This work was supported by the National Institutes of Health (grant number R01 CA16169401)

Acknowledgements

The authors would like to thank Patricia Egner of the Johns Hopkins Bloomberg School of Public Health for AFB1-DNA adduct measurements, Dr. Robert Rej of the

Molecular Diagnostics laboratory of Wadsworth Center for AST measurements, and Dr. Tom Friedrich of Albany Medical Center for resource assistance.

References

1. Shupe,T et al. (2004) Low hepatic glutathione-S-transferase and increased hepatic DNA adduction contribute to tumorigenicity of aflatoxin B1 in newborn and partially hepatectomized mice. Toxicol. Lett., 148, 1-9.

2. Eaton, D.L. et al. (1994) Mechanism of aflatoxin B1 carcinogenesis. Annu. Rev. Pharmacol. Toxicol., 34, 135-72, 1994.

3. Egner, P.A. et al. (2006) Quantification of aflatoxin-B1-N7-guanine in human urine by high-performance liquid chromatography and isotope dilution tandem mass spectrometry. Chem. Res. Toxicol., 19, 1191-1195.

4. Hayes J.D. et al. (1992) Molecular cloning and heterologous expression of a cDNA encoding a mouse glutathione S transferase Yc subunit possessing high catalytic activity for aflatoxin B1-8,9-epoxide. Biochem. J., 285, 173-180.

5. Hayes J.D. et al. (1994) Cloning of cDNAs from fetal rat liver encoding a mouse glutathione S-transferase Yc polypeptides. The Yc2 subunit is expressed in adult rat liver resistant to the hepatocarcinogen alfatoxin B1. J. Biol. Chem., 269, 20707-20717.

6. Vesselinovitch S et al. (1972) Mihailovich N, Wagon GN, Lombard LS, Rao KV. Aflatoxin B1, an hepatocarcinogen in the infant mouse. Cancer Res., 32, 2289-2291.

7. Ilic Z. et al. (2010) Glutathione-S-transferase A3 knockout mice are sensitive to acute cytotoxic and genotoxic effects of aflatoxin B1. Toxicol. & Applied Pharmacol., 242, 241-246.

8. Sell S. and Leffert HL. (2008) Liver Cancer Stem Cells. J. Clin. Oncol., 26, 2800-2805.

9. Sell S. et al. (1989) Evidence for the stem cell origin of hepatocellular carcinoma and cholangiocarcinoma. Am. J. Pathol., 134, 1347-1363.

10. Jelnes P. et al. (2007) Remarkable heterogeneity displayed by oval cells in rat and mouse models of stem cell-mediated liver regeneration. Hepatology, 45, 1462-70.

11. Bird T.G. et al. (2008) Activation of stem cells in hepatic diseases. Cell Tissue Res., 331, 283-300.

12. Tan E.K. et al. (2015) Liver injury models for induction of hepatic oval cells in rodents. J. Liver Res. Disord. Ther., 1(1), 00005.

13. Alison M.R. et al. (2005) Liver stem cells. Implications for hepatocarcinogenesis. Stem Cell Reviews, 1, 253-260.

14. Rutenburg A.M. et al. (1969) Histochemical and ultrastructural demonstration of γ-glutamyl transpeptidase activity. J. Histochem. Cytoschem., 17, 517-526.

15. Milne G.L. et al. (2013) Measurement of F2-isoprostanes and isofurans using gas chromatography-mass spectrometry. Free Radic. Biol. Med., 59, 36-44.

16. Chanas S.A. et al. (2002) Loss of the Nrf2 transcription factor causes a marked reduction in constitutive and inducible expression of the glutathione S-transferase Gsta1, Gsta2, Gstm1, Gstm2, Gstm3 and Gstm4 genes in the livers of male and female mice. Biochem. J., 365, 405-16.

17. Bergmeyer H.U. et al. (1986) Approved Recommendation (1985) on IFCC methods for the measurement of catalytic concentration of enzymes. Part 2. IFCC Method for aspartate aminotransferase. J. Clin. Chem. Clin. Biochem., 24, 497-510.

18. Becker F.F. (1982) Morphological classification of mouse liver tumors based on biological characteristics. Cancer Res., 42, 3918-3923.

19. Zhou S.F. et al. (2009) Insights into the substrate specificity, inhibitors, regulation, and polymorphisms and the clinical impact of human cytochrome P450 1A2. AAPS J., 11, 481-94.

20. Martignoni M. et al. (2006) Species differences between mouse, rat, dog, monkey and human CYP-mediated drug metabolism, inhibition and induction. Expert Opinion on Drug Metabolism & Toxicology, 2, 875-94.

21. Tiemersma E.W. (2001) Role of genetic polymorphism of glutathione-S-transferase T1 and microsomal epoxide hydrolase in aflatoxin-associated hepatocellular carcinoma. Cancer Epidemiol. Biomark. Prev., 10, 785-791.

22. Kensler K.H. (2014) Genetic or pharmacologic activation of Nrf2 signaling fails to protect against aflatoxin genotoxicity in hypersensitive GSTA3 knockout mice. Toxicol. Sci., 139, 293-300.

23. Wu H.C. et al. (2007) Urinary 8-oxodeoxyguanosine, aflatoxin B-1 exposure and hepatitis B virus infection and hepatocellular carcinoma in Taiwan. Carcinogenesis, 28, 995–999.

24. Guindon K.A. et al. (2008) Failure of catalase to protect against aflatoxin B1-induced mouse lung tumorigenicity. Toxicol. Appl. Pharmacol., 227, 179-183.

25. Lin W.C. (2006) Inhibitory effect of CDA-II, a urinary preparation, on aflatoxin B(1)-induced oxidative stress and DNA damage in primary cultured rat hepatocytes. Food Chem. Toxicol., 44, 546-551.

26. Yang Y. et al. (2002) Role of alpha class glutathione S-transferases as antioxidant enzymes in rodent tissues. Toxicol Appl Pharmacol., 182, 105-115.

27. Dwivedi S. et al. (2006) The course of CCl4 induced hepatotoxicity is altered in mGSTA4-4 null (-/-) mice. Toxicology, 218, 58-66.

28. Wogan G.N. et al. (1971) Structure-activity relationships in toxicity and carcinogenicity of aflatoxins and analogs. Cancer Res., 31, 1936-1942.

29. Johnson N.M et al., (2014) Complete protection against aflatoxin B1-induced liver cancer with triterpenoid: DNA adduct dosimetry, molecular signature and genotoxicity threshold. Cancer Prev. Res., 7, 658-665.

30. Moore M.R. et al. (1982) Cholangiocellular carcinomas in duced in Syrian golden hamsters administered aflatoxin B1 in large doses. J. Natl. Cancer Inst., 68, 271-278.

31. Piscaglia A.C. et al. (2009) Establishment of cancer cell lines from rat hepatocholangiocarcinoma and assessment of the role of granulocyte-colony stimulating factor and hepatocyte growth factor in their growth, motility and survival. J. Hepatol., 51, 77-92.

32. Elmore L.W. and Sirica A.E. (1991) Phenotypic characterization of metaplastic intestinal glands and ductular hepatocytes in cholangiofibrotic lesions rapidly induced in the caudate liver lobe of rats treated with furan. Cancer Res., 51, 5752-5759.

33. Zhang F. et al. (2015) Expression and activation of EGFR and STAT3 during the multistage carcinogenesis of intrahepatic cholangiocarcinoma induced by 3’-methyl-4dimethylaminobenzene in rats. J. Toxicol. Pathol., 28, 79-87.

34. Fan L. et al. (2012) Bmi1 is required for hepatic progenitor cell expansion and liver tumor development. PLoS One, 7, e46472.

35. Lee J-H. et al. (1997) Heterogeneity of the “oval-cell” response in the hamster liver during cholangiocarcinogenesis following Clonorchis sinensis infection and dimethylnitrosamine treatment. J. Hepatol., 26, 1313-1323.

36. Zhang F. et al. (2008) Combined hepatocellular cholangiocarcinoma originating from hepatic progenitor cells: immunohistochemical and double-fluorescence immunostaining evidence. Histopathology, 52, 224-232.

37. Sempoux C. et al. (2011) Cholangiocellular carcinoma: an innocent-looking malignant liver tumor mimicking ductular reaction. Semin. Liver Dis., 31, 104-110.

38. Preisseger K-H. et al. (1999) Atypical ductular proliferation and its inhibition by TGF beta1 in the DDC mouse model for chronic alcoholic liver disease. Lab. Invest., 79, 103-109.

39. Petersen B.E. et al. (2003) Mouse A6-positive hepatic oval cells also express several hematopoietic stem cell markers. Hepatology, 37, 632-640.

40. Akhurst B. et al. (2001) A modified choline-deficient, ethionine-supplemented diet protocol effectively induces oval cells in mouse liver. Hepatology, 34, 515-522.

41. Marchand-Strick H. et al. (2008) Lymphocytes support oval cell-dependent liver regeneration. J. Immunol., 181, 2764-2771.

42. Jowsey I.R. et al. (2003) Expression of the aflatoxin B1-8,9-epoxide-metabolizing murine glutathione S-transferase A3 subunit is regulated by the Nrf2 transcription factor through an antioxidant response element. Mol. Pharmacol., 64, 1018-1028.

43. Storz G. et al. (1987) Spontaneous mutagenesis and oxidative damage to DNA in Salmonella typhimurium. Proc. Natl. Acad. Sci. U.S.A., 84, 8917-8921.

44. Cerutti P.A. et al. (1991) Inflammation and oxidative stress in carcinogenesis. Cancer Cells 3, 1-7.

45. Halliwell B. et al. (1999) Free Radicals in Biology and Medicine, 3rd ed. Oxford University Press, NY, NY.

46. Martinez-Hernandez A. (1985) The hepatic extracellular matrix. II. Electron and immunohistological studies in rats with CCl4-induced cirrhosis. Lab. Invest., 53, 166-186.

47. Yin L. et al. (2002) Proliferation and differentiation of ductular progenitor cells and littoral ells during the regeneration of the rat liver to CCl4/s-AAF injury. Histol. Histopathol., 17, 65-81.

48. Hosoda A. et al. (1993) Effects of liver damage induced by carbon tetrachloride on glutathione and glutathione-dependent enzymes in rat gastric mucosa. Res. Comm. Chem. Pathol. Pharmacol., 79, 141-150.

49. Engle M.R. et al. (2004) Physiological role of mGSTA4-4, a glutathione S-transferase metabolizing 4-hydroxynonenal: a generation and analysis of mGsta4 null mouse. Toxicol. Appl. Pharmacol., 194, 296-308.

50. Csala M. et al. (2015) On the role of 4-hydroxynonenal in health and disease. Biochim. Biophys. Acta, 1852, 826-38.

Table 1. F_2-isoprostane, isofuran and AST levels in male and female wild type and GSTA3 knockout mice following exposure to carbon tetrachloride

Marker	CCl_4 (hrs)	Male		Female	
		WT	KO	WT	KO
Isoprostane	0	2.26 +/- 0.20	2.41 +/- 0.26	1.70 +/- 0.03	3.23 +/- 0.12*,**
	2 hours	50.70 +/- 2.66	53.69 +/- 2.28	51.46 +/- 4.61	56.58 +/- 4.7
	8 hours	7.87 +/- 1.17	9.44 +/- 0.85	6.05 +/- 0.34	10.42 +/- 0.86*
	24 hours	2.51 +/- 0.08	2.54 +/- 0.27	3.48 +/- 0.32	5.47 +/- 1.19**
Isofuran	0	2.82 +/- 0.13	2.73 +/- 0.29	2.05 +/- 0.13	3.28 +/- 0.21*
	2 hours	17.89 +/- 1.55	21.16 +/- 2.02	18.89 +/- 2.09	22.50 +/- 1.49
	8 hours	5.82 +/- 0.45	9.26 +/- 0.92*	3.36 +/- 0.09	5.31 +/- 0.55*,**
	24 hours	3.04 +/- 0.20	2.19 +/- 0.24	2.96 +/- 0.46	4.47 +/- 0.82**
AST	0	176 +/- 26	217 +/- 32	221 +/- 39	250 +/- 37
	2 hours	264 +/- 23	202 +/- 23	214 +/- 46	475 +/- 135**
	8 hours	670 +/- 204*	489 +/- 65*	693 +/- 34*	848 +/- 173*
	24 hours	3683 +/- 1117*	2494 +/- 1062*	3327 +/- 716*	3552 +/- 661*

F_2-isoprostane and isofuran data are expressed as ng/g liver tissue, and AST as units/liter serum. All data are presented as means +/- SEM (N=5-7). * Significant difference between WT and KO at each given time point when comparing F_2-isoprostane and isofuran data, and significant difference between Control and 8 hour or 24 hour time points when comparing AST data, both using a 2-tailed Student's *t*- test at $p<0.05$. ** Significant difference between male and female KO at each given time point using a 2-tailed Student's *t*- test at $p<0.05$.

Figure legends

Figure 1. Gross (A-D) and microscopic (E-L) lesions in GSTA3 KO mice treated with weekly (12 or 24) AFB1 injections (0.5 mg/kg). A. Normal (control) liver, male mouse, 24 injections of vehicle (DMSO) (L, M, R, C – left, middle, right and caudate lobes). **B.** Cysts (short arrows in middle lobe) and tumor (long arrow in left lobe), male, 12 injections. **C.** Multiple nodules (short arrows) and tumors (long arrows in left and right), male, 24 injections. **D.** Entire liver composed of coalescing nodules (arrows), female, 24 injections. **E, F.** Multifocal cholangiomas (arrows), male, 24 injections, H&E (40X). Cholangioma in **F** is a higher magnification (200X) of a rectangle in **E**. **G.** Cholangiocarcinoma (arrows), female, 24 injections, H&E (200X). **H, I.** Becker type 1 hepatocellular nodule (arrows), female, 24 injections, H&E (40X). **I** is a higher magnification (200X) of a rectangle in **H**. **J.** Pan-CK positive cholangioma cells (arrows), female, 24 injections (200X). **K.** Mucicarmine stained mucin in cholangiocarcinoma, male, 24 injections (200X). **L.** GGT positive focus of hepatocytes (arrow), female, 12 injections (40X). **M.** GST-P stained small focus of hepatocytes (arrow) and individual cells, female, 24 injections (200X).

Figure 2. Histologic effects of AFB1 treatment (0.5 mg/kg) in GSTA3 KO mice. A-H; H&E stained images. **A.** Liver of a male mouse given DMSO once a week for 13 weeks (200X). **B-H** livers after weekly injections of 0.5 mg/kg AFB1. **B.** Grade 2 OC proliferation extends to mid-zone (200X). **C.** Grade 4 OC proliferation extends from

portal (P) to central (C) zone (200X). **D.** Microvesicular fatty change (200X). **E.** Megahepatocytes (examples shown with arrows) (200X). **F.** Nuclear inclusions (examples shown with arrows) (400X). G. Cholangiomas (200X). **H.** Nodule (Becker grade I) (40X).

Figure 3. Oval cell proliferation in liver in response to acute AFB1 exposure (1 mg/kg). A-F and **I**; H&E staining. **G** and **H**; A6 and Pan-CK immunostaining, respectively. **A.** KO female mouse liver, untreated. P=portal vein branch, C=central vein branch (200X). **B.** KO female mouse, 5 days after AFB1. Acute injury with cell necrosis and swelling visible (100X). **C, D.** KO female mouse, 10 days after AFB1. Numerous oval cells are visible (arrows in D). **D** is a higher magnification (400X) of the dashed line rectangle in C (200X). **E.** KO female mouse, 15 days after AFB1. Oval cells are seen throughout the lobule (arrows) (200X). **F.** KO female mouse, 30 days after AFB1. Numerous oval cells are still present (arrows) (200X). **G.** KO female mouse, 15 days after AFB1. Oval cells are A6-positive (arrows) (200X). **H.** KO female mouse, 30 days after AFB1. Oval cells are Pan-CK-positive (arrows) (200X). **I.** KO male mouse, 10 days after AFB1. No oval cells are seen at any time after AFB1 (200X).

Figure 4. AFB1-DNA adduct formation in liver in response to acute AFB1 exposure. Mice were given 0.87 mg/kg AFB1 in DMSO or DMSO only (control) by gavage, and livers collected 2 hours later. **WT-F**, wild type female; **WT-M**, wild type male; **KO-F**, knockout female; **KO-M**, knockout male. Data are expressed as mean ± SEM (N=5). *Significant difference using a two-tailed Student's t-test at $p<0.05$.

Figure 5. Gender and genotype comparison of GSTs and aflatoxin metabolizing proteins. Four groups of three month old C57Bl/6J mice representing WT males, WT females, KO males, and KO females (7 animals for each group) were sacrificed and livers removed and extracts prepared. For GST isoform analyses, these extracts were further chromatographed on a glutathione affinity column. Equal amounts of purified GST-containing proteins (A-E) or extracts (F-H) were then electrophoresed and analyzed by Western immunoblotting. **A.** GSTA3; **B.** GSTP1; **C.** GSTM1; **D.** GSTM5; **E.** GSTA4; **F.** CYP1A2; **G.** CYP3A11; **H.** epoxide hydrolase. Blots were then stripped and reprobed with- and data normalized to- VDAC1 loading control. Quantitation of blot signals was carried out using ImageJ. **I.** GST activity in WT and KO mouse livers. Samples were prepared as described above and GST enzyme activity measured in the affinity purified extracts. White plot, wild type mice; grey plot, knockout mice. Data are expressed as mean ± SEM (N=7). *Significant difference using a two-tailed Student's t-test at $p<0.05$.

Fig. 1A-D

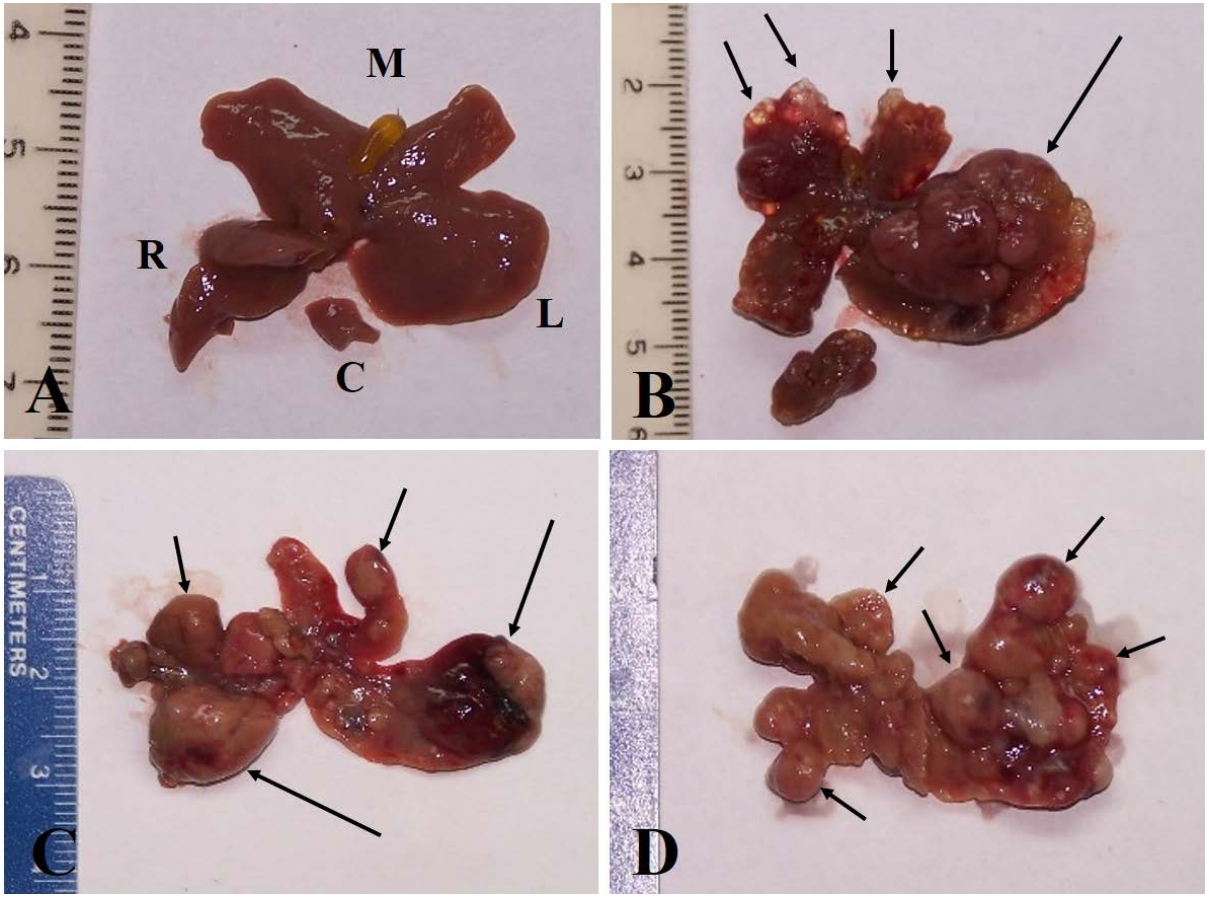

Fig. 1E-L

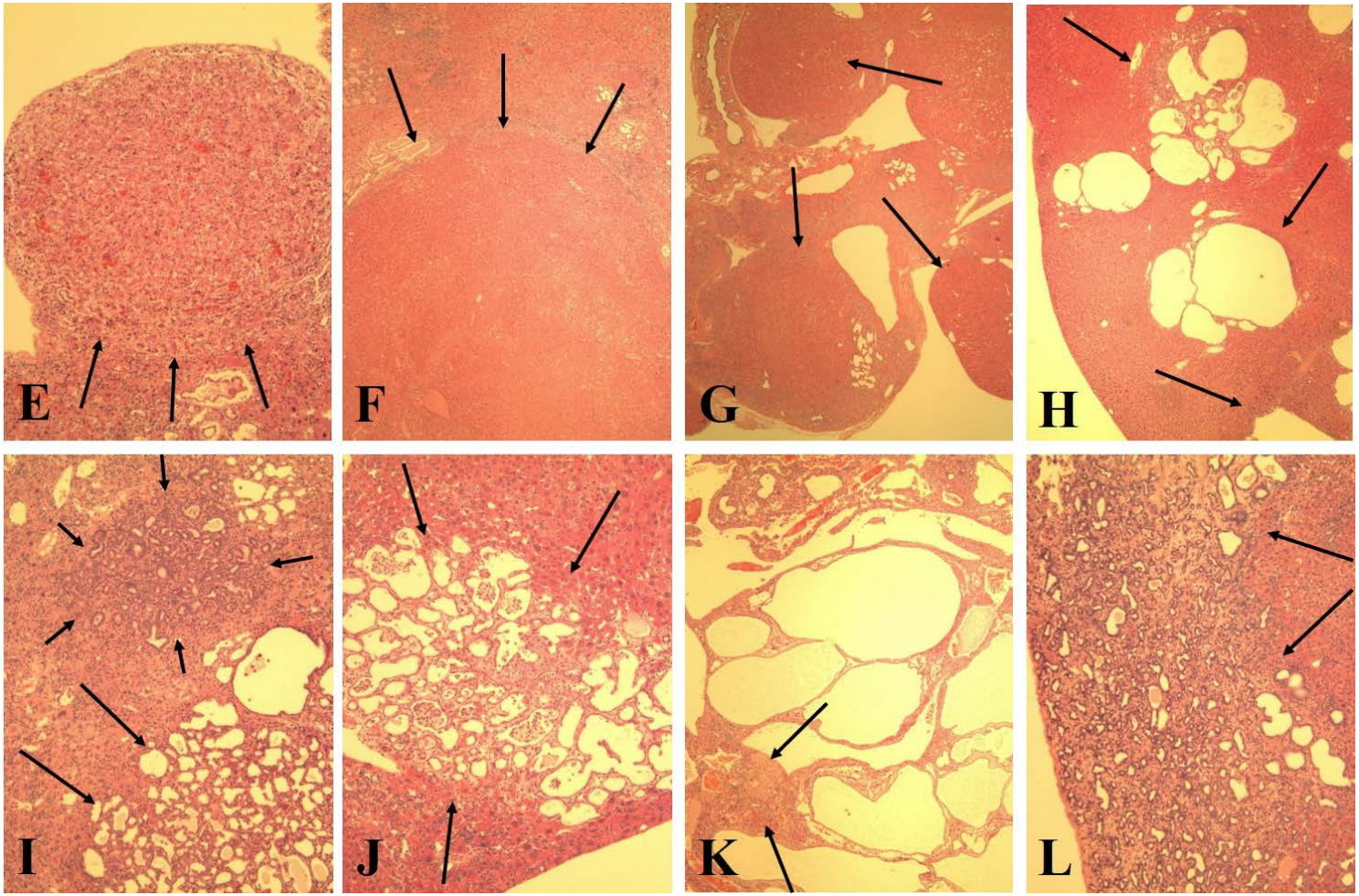

Fig. 2

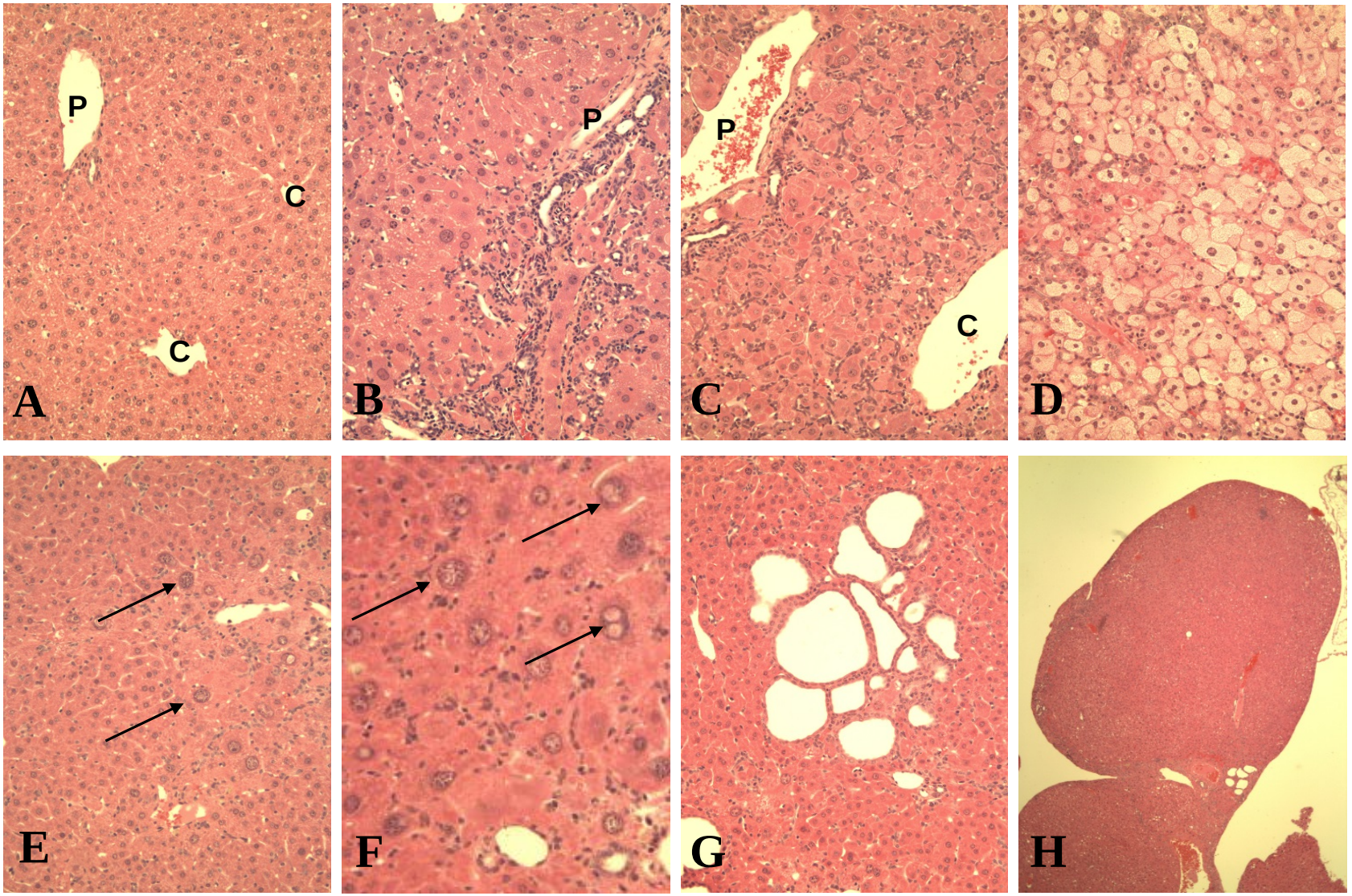

Fig. 3

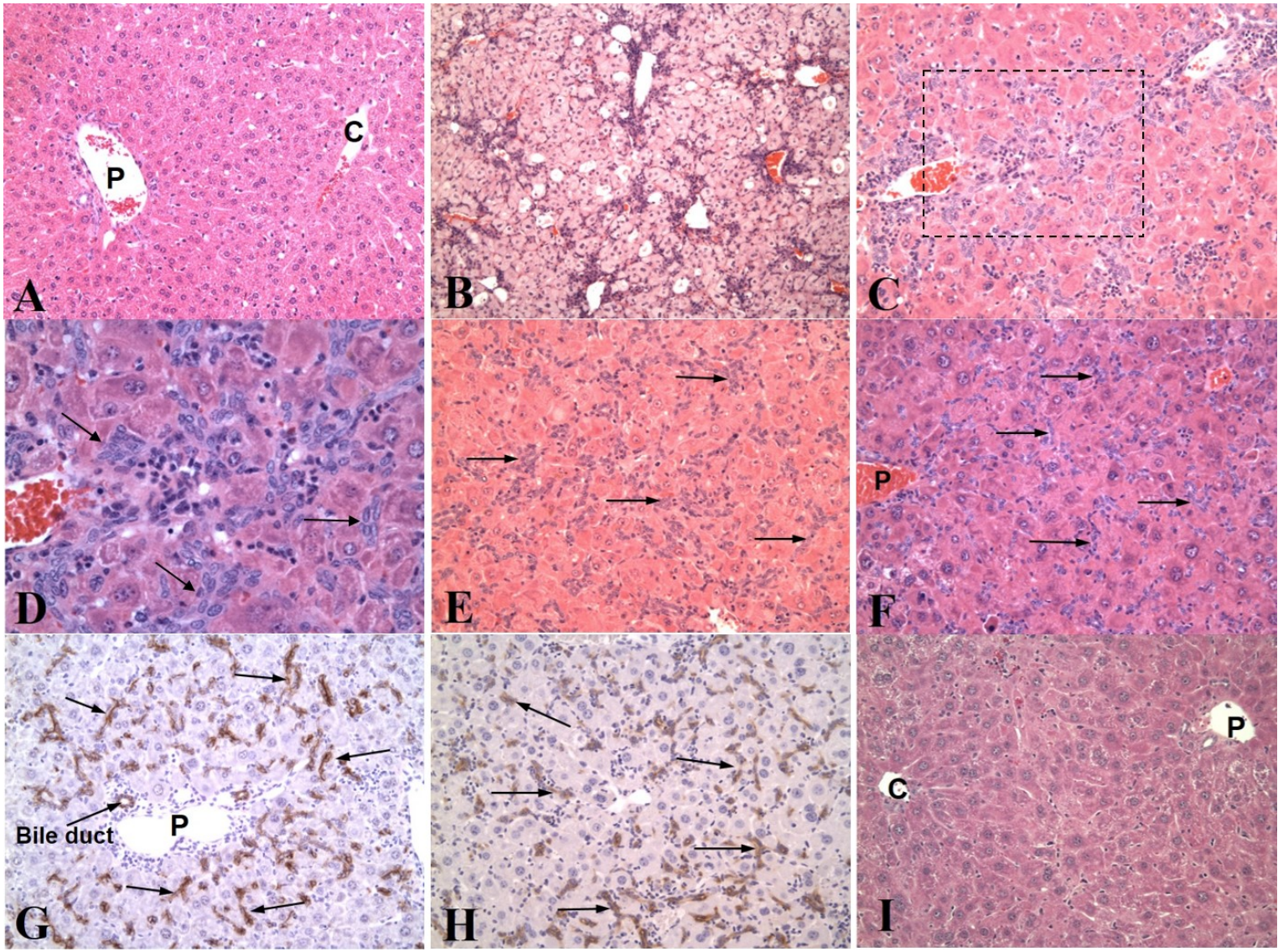

Fig. 4

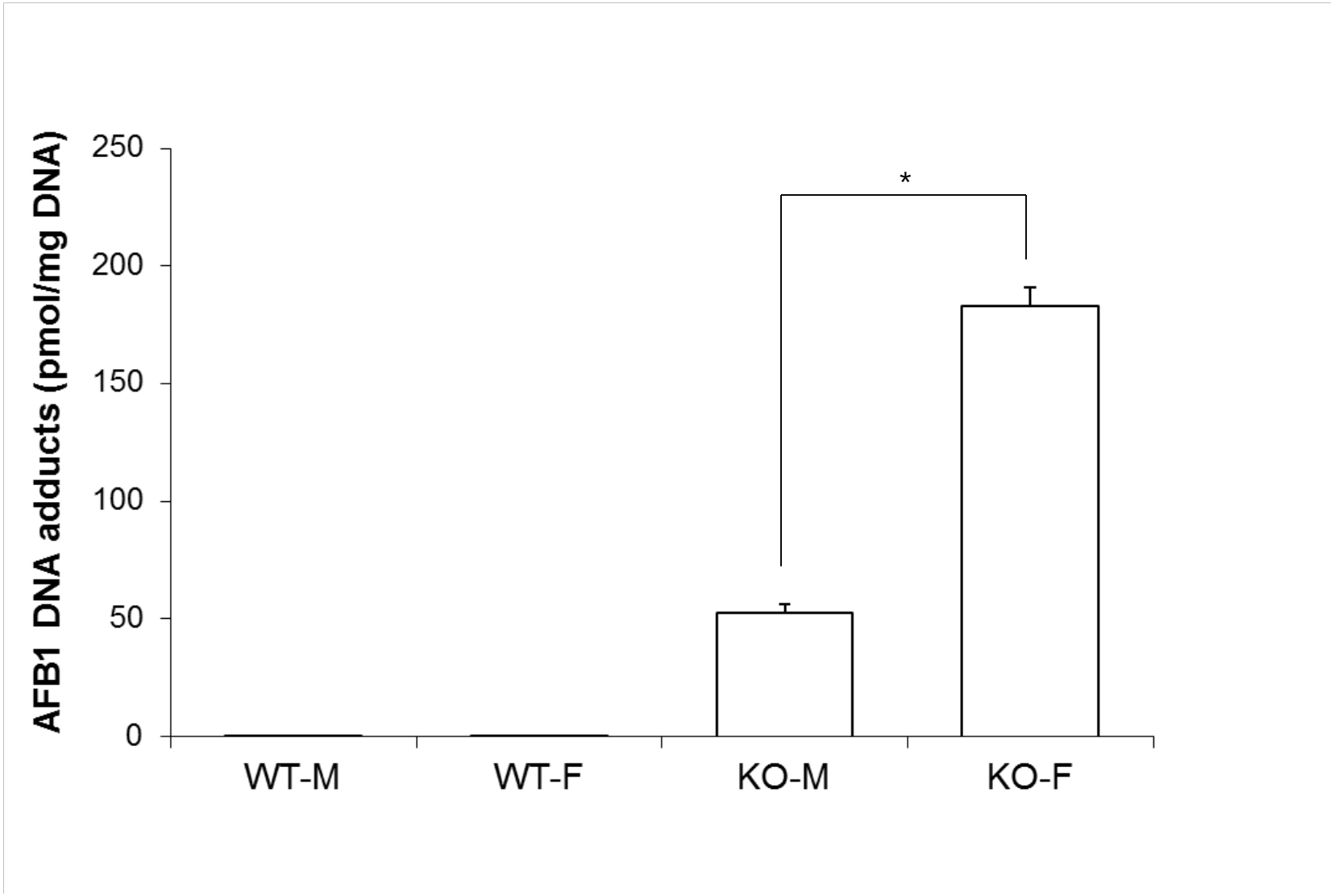
AFB1 DNA adducts (pmol/mg DNA)
250
200
150
100
50
0
*
WT-M
WT-F
KO-M
KO-F

Fig. 5A

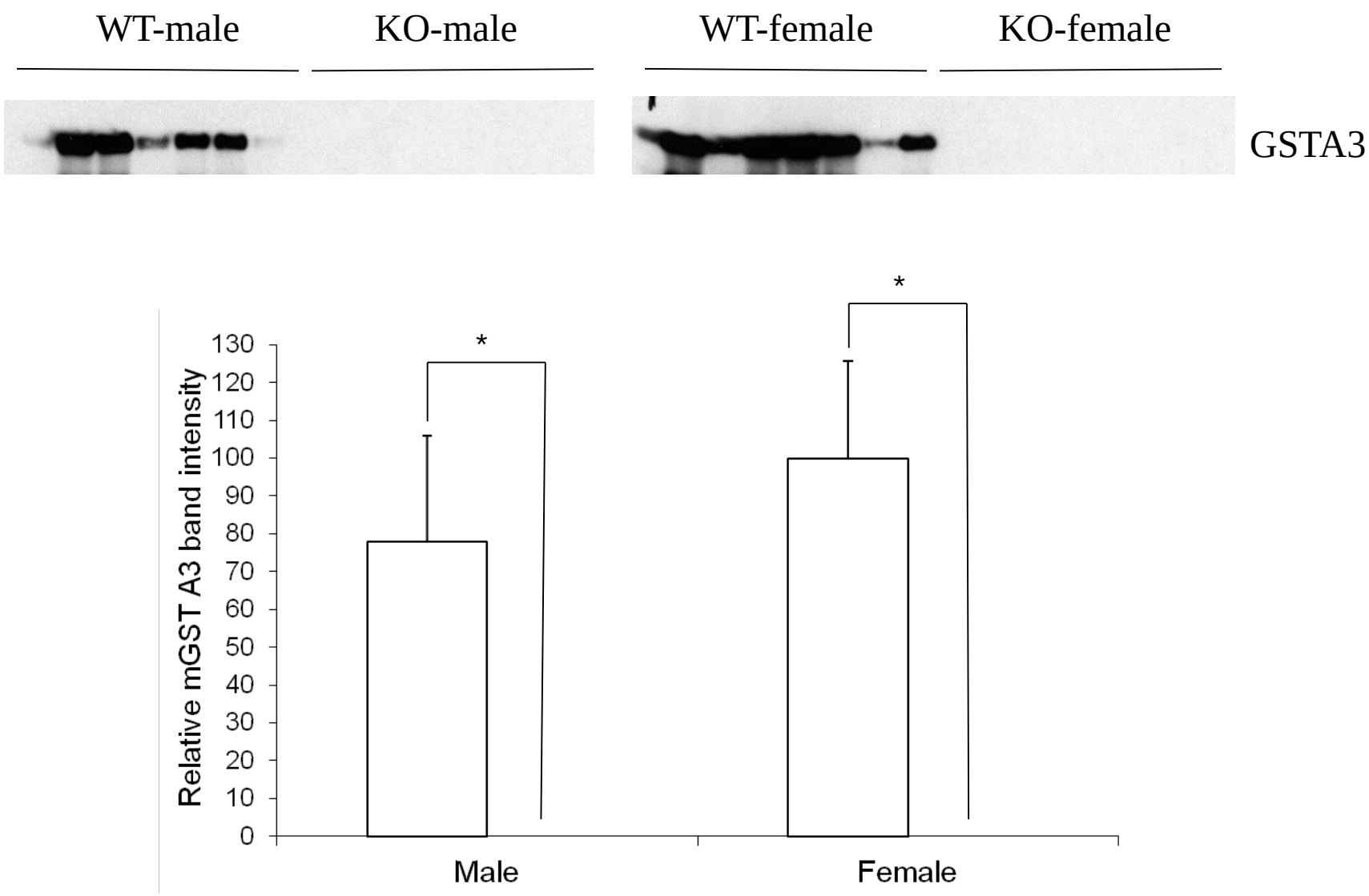
WT-male
KO-male
WT-female
KO-female
GSTA3
Relative mGST A3 band intensity
130
120
110
100
90
80
70
60
50
40
30
20
10
0
*
*
Male
Female

Fig. 5B

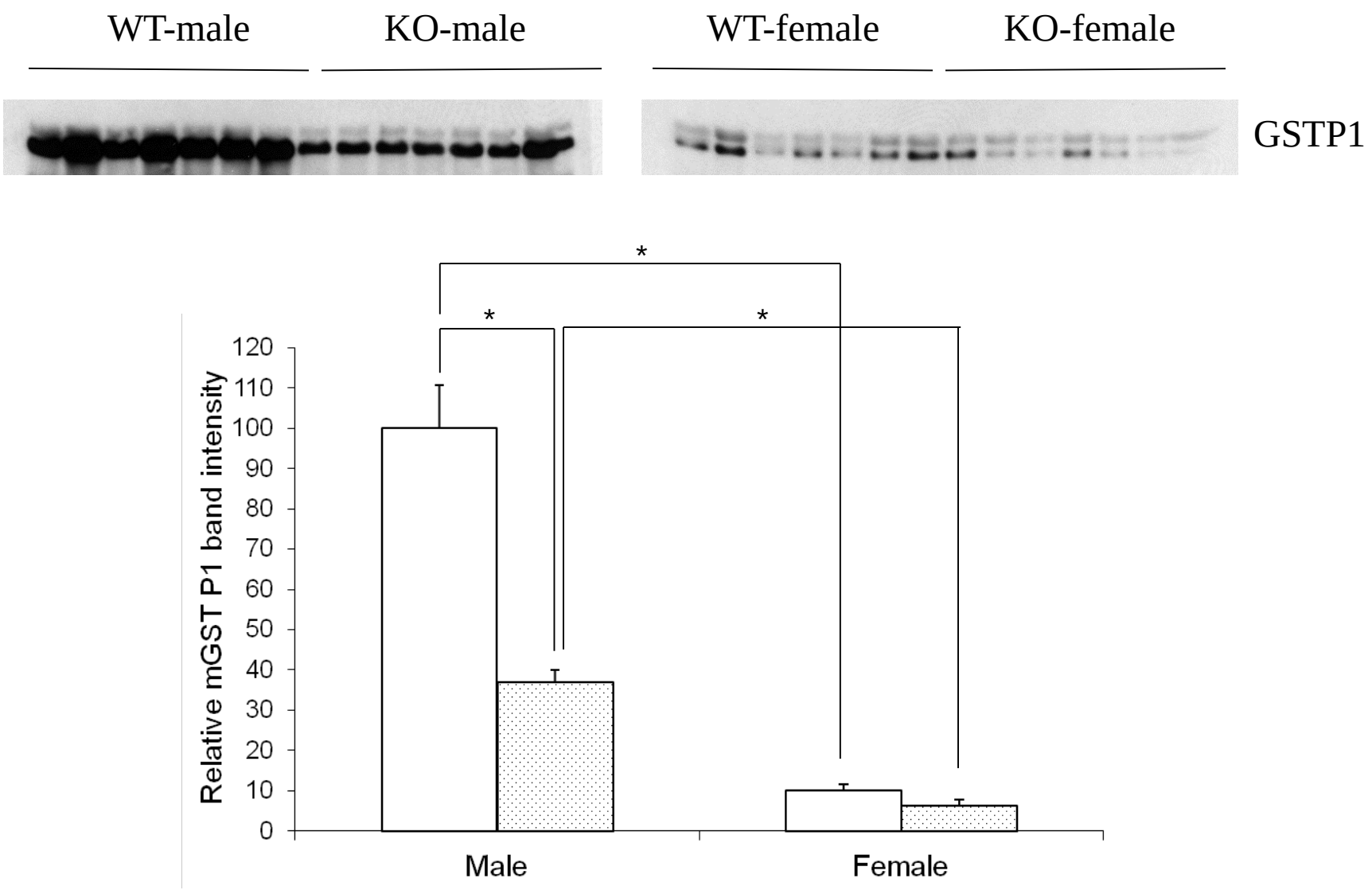
WT-male
KO-male
WT-female
KO-female
GSTP1
*
*
*
Relative mGST P1 band intensity
120
110
100
90
80
70
60
50
40
30
20
10
0
Male
Female

Fig. 5C

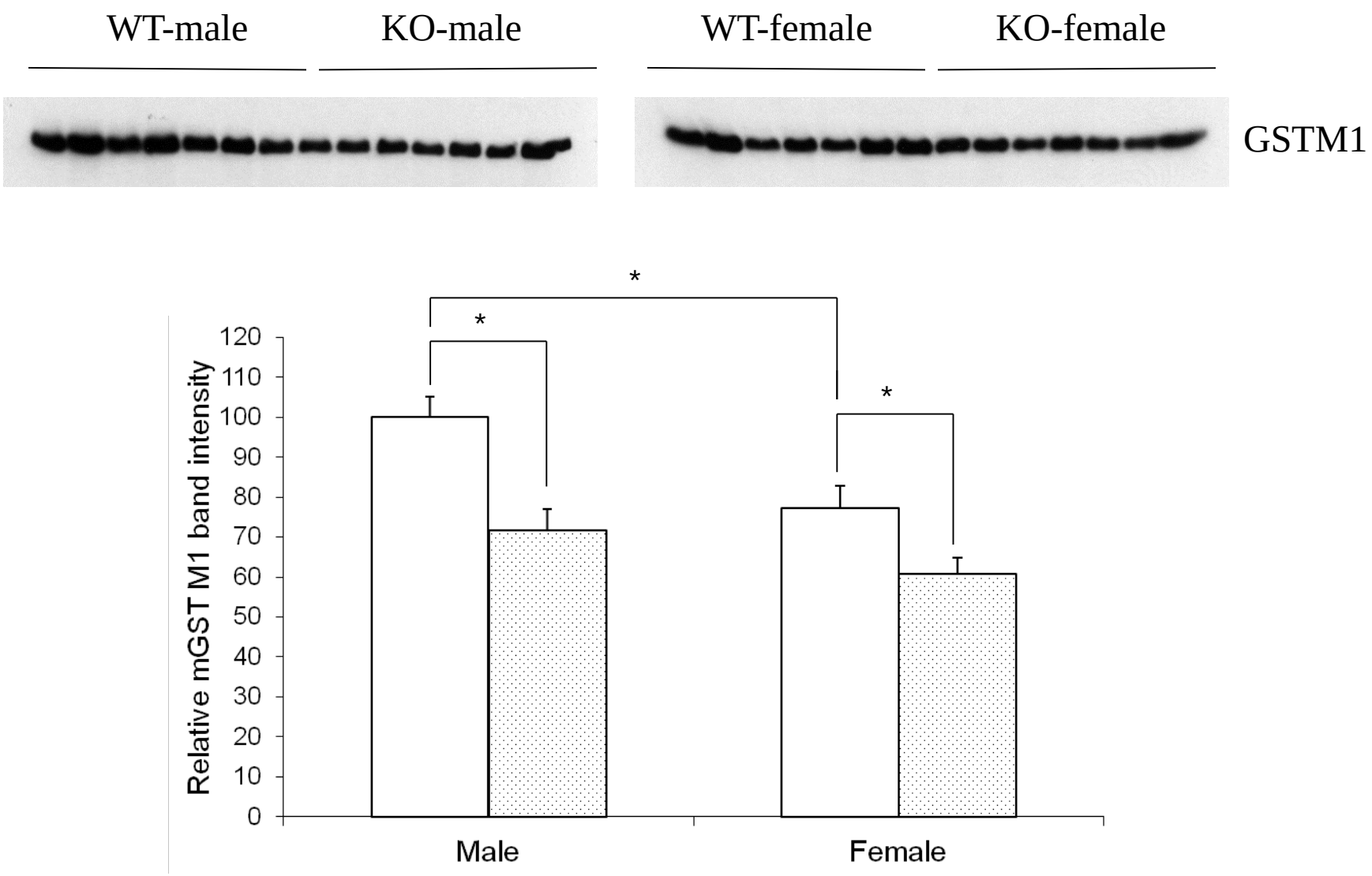
WT-male
KO-male
WT-female
KO-female
GSTM1
Relative mGST M1 band intensity
120
110
100
90
80
70
60
50
40
30
20
10
0
*
*
*
Male
Female

Fig. 5D

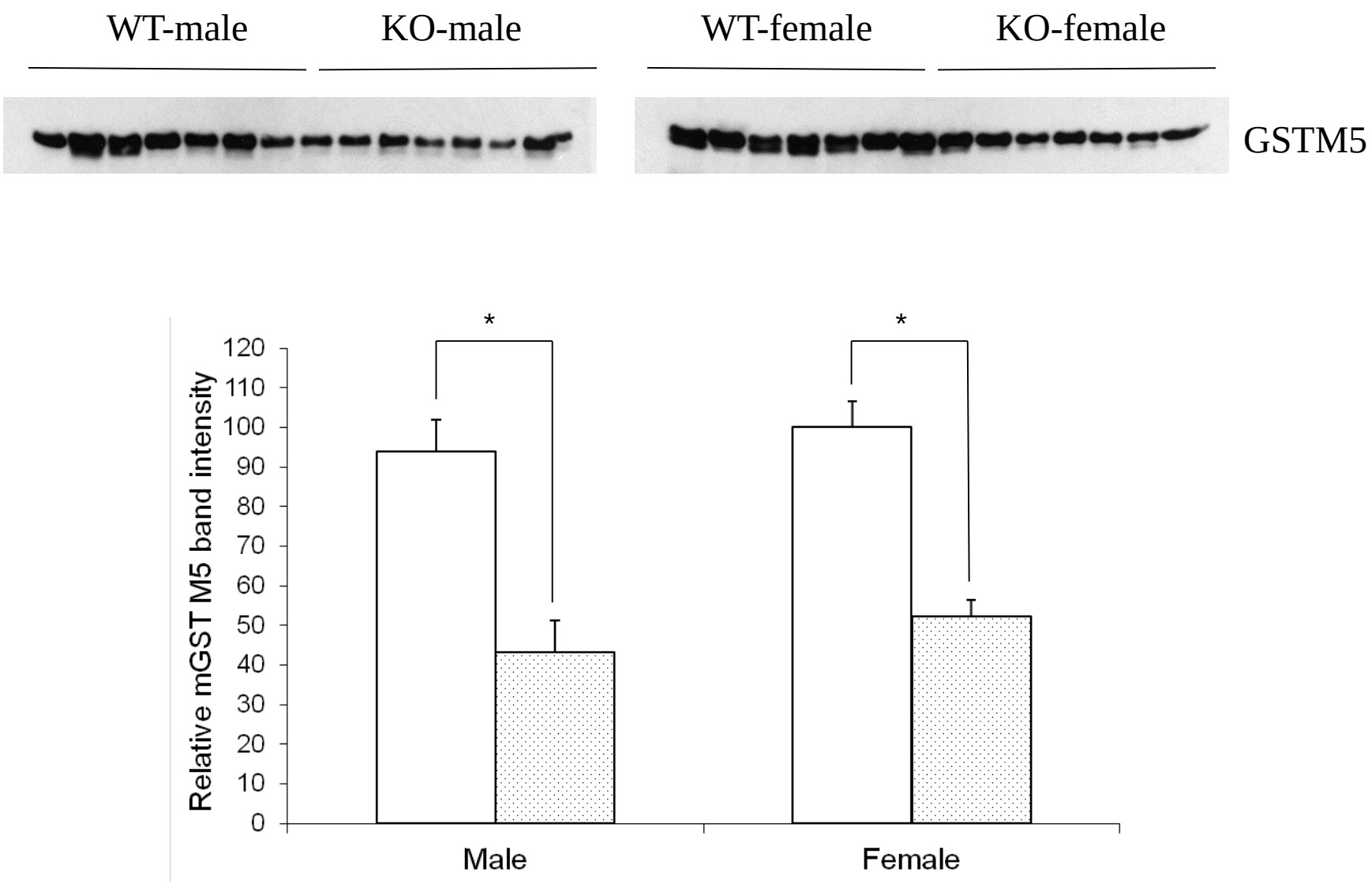
WT-male
KO-male
WT-female
KO-female
GSTM5
Relative mGST M5 band intensity
120
110
100
90
80
70
60
50
40
30
20
10
0
*
*
Male
Female

Fig. 5E

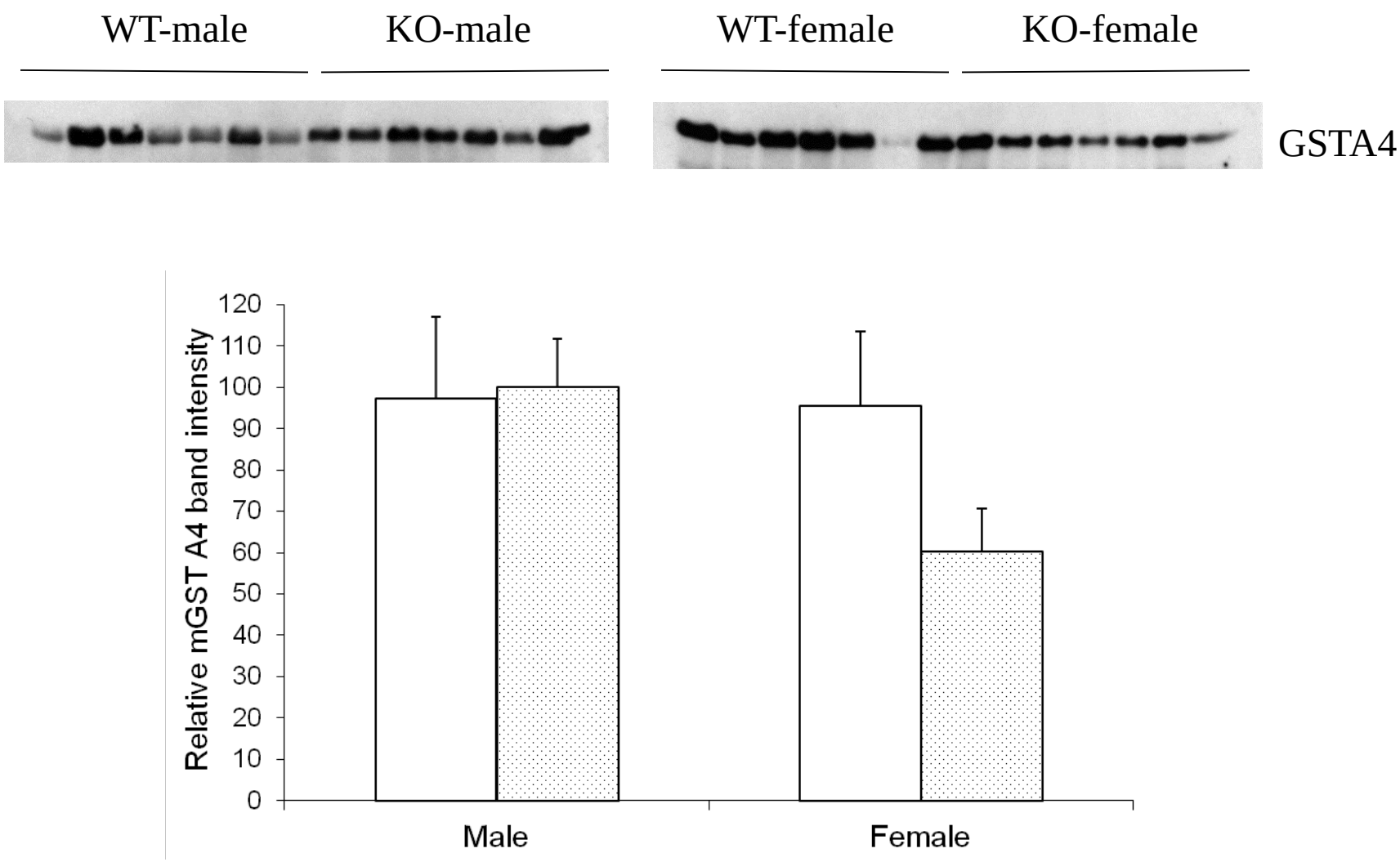
WT-male
KO-male
WT-female
KO-female
GSTA4
Relative mGST A4 band intensity
120
110
100
90
80
70
60
50
40
30
20
10
0
Male
Female

Fig. 5F

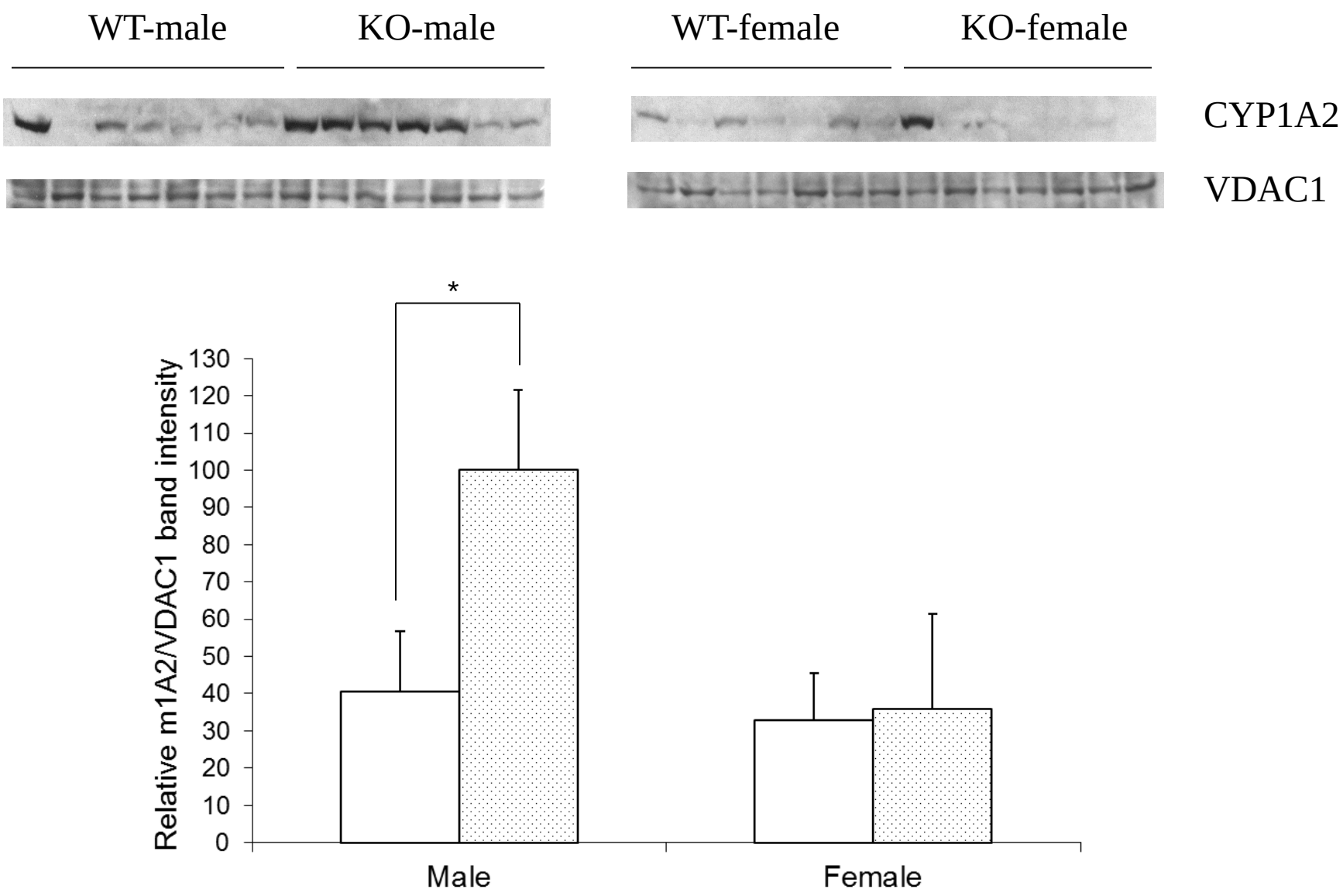
WT-male
KO-male
WT-female
KO-female
CYP1A2
VDAC1
*
Relative m1A2/VDAC1 band intensity
130
120
110
100
90
80
70
60
50
40
30
20
10
0
Male
Female

Fig. 5G

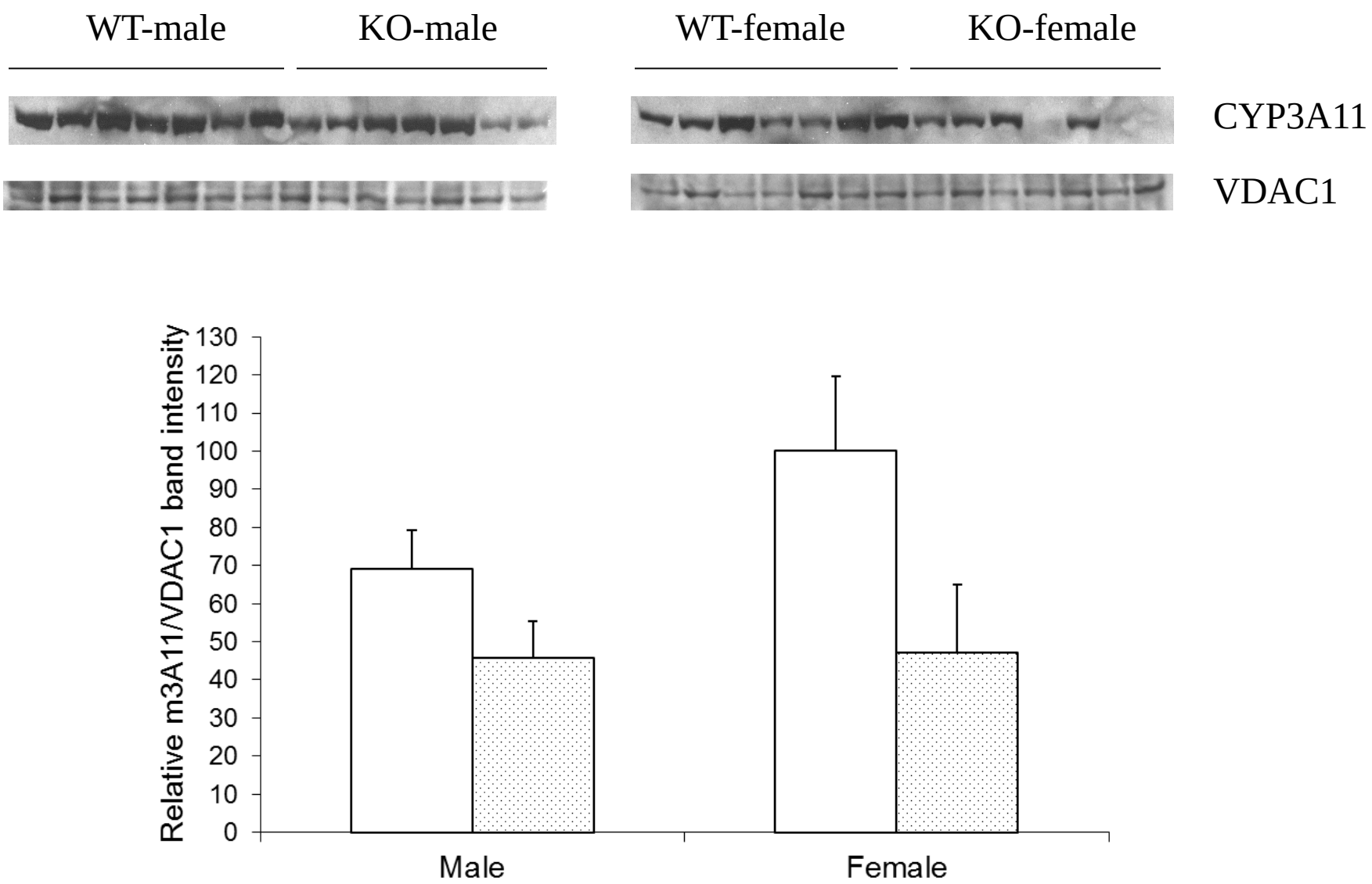
WT-male
KO-male
WT-female
KO-female
CYP3A11
VDAC1
Relative m3A11/VDAC1 band intensity
130
120
110
100
90
80
70
60
50
40
30
20
10
0
Male
Female

Fig. 5H

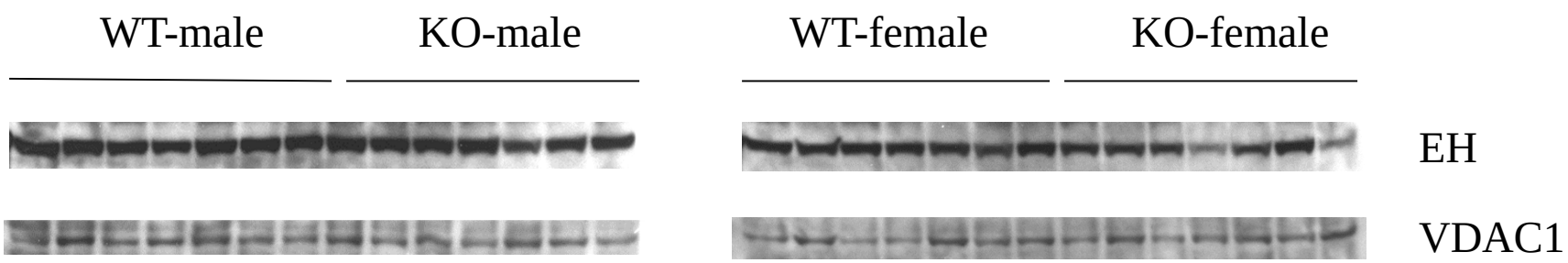
WT-male
KO-male
WT-female
KO-female
EH
VDAC1

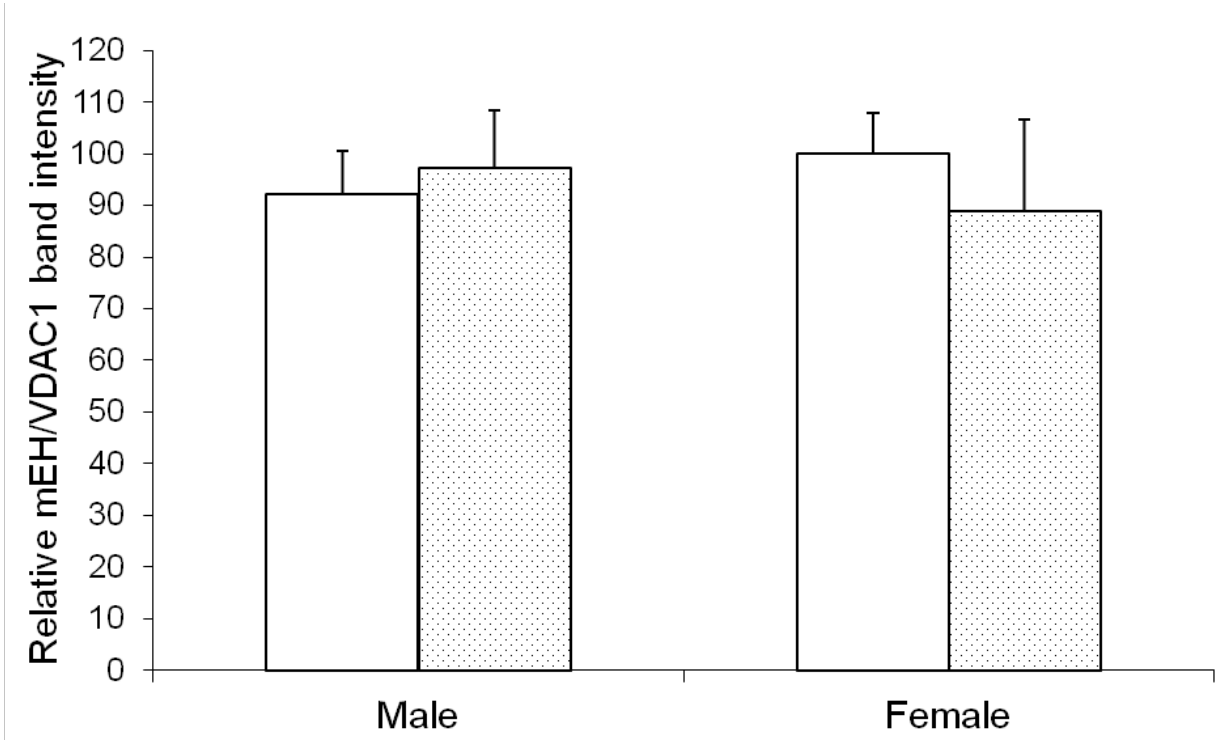
Relative mEH/VDAC1 band intensity
120
110
100
90
80
70
60
50
40
30
20
10
0
Male
Female

Fig. 5I

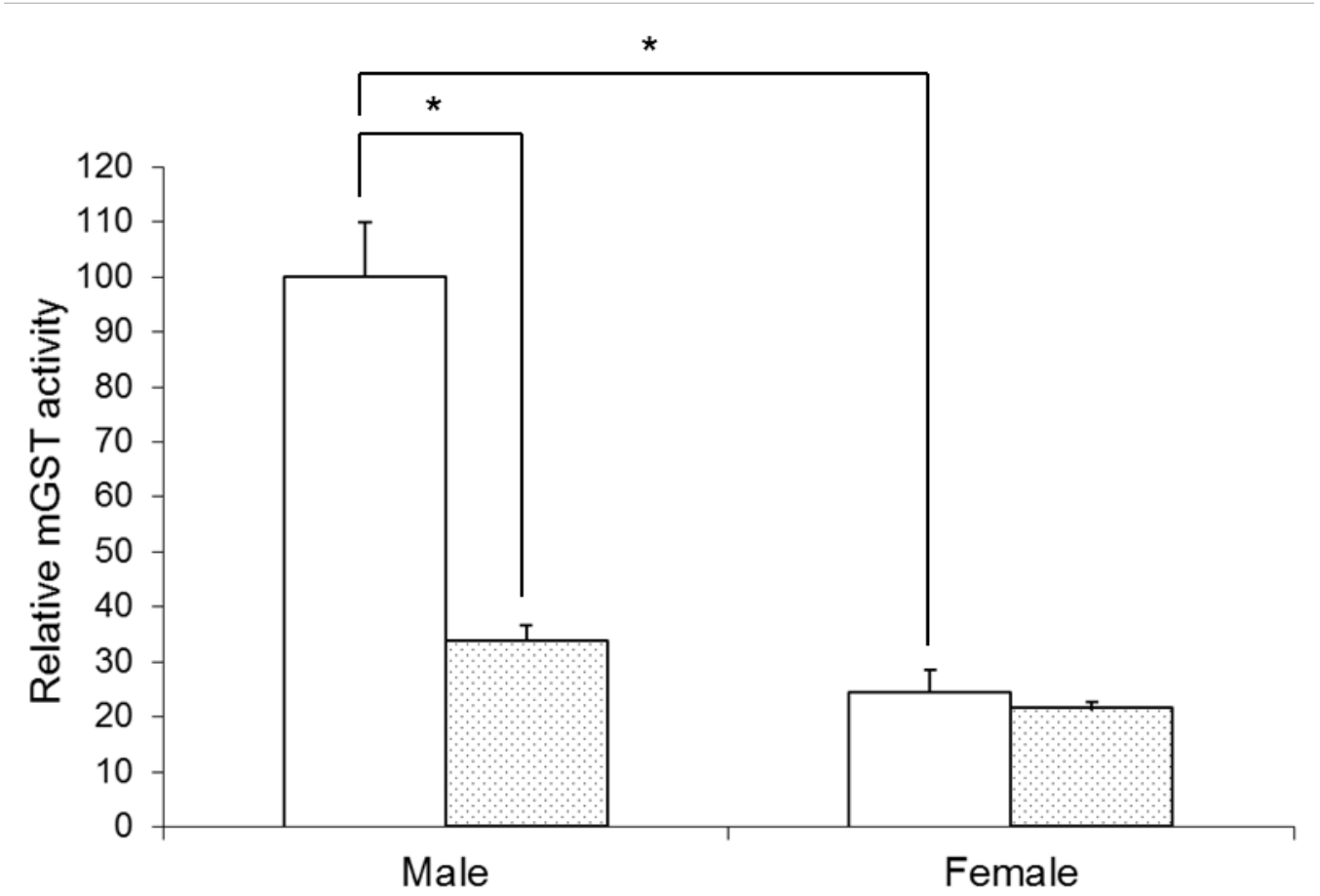
*
*
120
110
100
90
80
70
60
50
40
30
20
10
0
Relative mGST activity
Male
Female